ACSNANO

www.acsnano.org

ARTICLE

Glucose-Activated Nanoconfinement Supramolecular Cascade Reaction *in Situ* for Diabetic Wound Healing

Lei Chen, Yong Chen, Rong Zhang, Qilin Yu, Yong Liu, and Yu Liu*

Cite This: https://doi.org/10.1021/acsnano.2c04566

Read Online

ACCESS | Metrics & More | Article Recommendations | Supporting Information

ABSTRACT: Supramolecular nanofunctional materials have attracted increasing attention from scientific researchers due to their advantages in biomedicine. Herein, we construct a nanosupramolecular cascade reactor through the cooperative interaction of multiple noncovalent bonds, which include chitosan, sulfobutylether-β-cyclodextrin, ferrous ions, and glucose oxidase. Under the activation of glucose, hydroxyl radicals generated from the nanoconfinement supramolecular cascade reaction process are able to initiate the radical polymerization process of vinyl monomers to form hydrogel network structures while inhibiting resistant bacterial infection. The results of the diabetic wound experiment confirmed the capacity of the glucose-activated nanoconfinement supramolecular cascade reaction *in situ* for potent antimicrobial efficacy and wound protection. This strategy of "two birds with one stone" provides a convenient method for the application of supramolecular nanomaterial in the field of biomedicine.

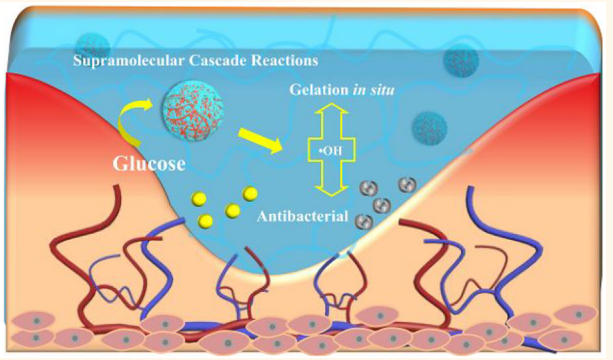

KEYWORDS: *sulfobutylether-β-cyclodextrin, supramolecular cascade reactor, diabetes chronic wound, antibacterial, hydrogel*

INTRODUCTION

Since the formation of supramolecular nanofunctional materials via a supramolecular chemical strategy enables the efficient integration of diverse bioactive species, supramolecular nanofunctional materials are widely applied in the field of biomedicine, such as in diabetes mellitus treatment,[1−3] targeted drug delivery, and tumor therapy.[4−7] Recently, supramolecular nanoconfined catalytic material that can mimic the human immune system to produce reactive oxygen species (ROS) has been effectively applied against bacterial infection.[8] Specifically, species with high peroxidase- or oxidase-like catalytic activities in supramolecular systems are able to generate ROS such as hydroxyl radicals (·OH) through the catalytic hydrogen peroxide (H_2O_2) decomposition process. To further locally replenish the concentration of H_2O_2 at the infection site as well as to avoid the damage of external added H_2O_2 to normal tissues, a glucose-assisted cascade catalytic supramolecular system was developed.[9] For instance, a MOF-based hybrid nanocatalyst as a benign and self-activated cascade reagent is constructed by Qu, which exhibits potent antibacterial efficacy through the self-activation of the peroxidase-like activity process by glucose oxidation.[10]

Due to multiple complications resulting from diabetes mellitus, bacterial infections in diabetic patient wounds can cause immense suffering, such as diabetic ulcers and diabetes-related amputations.[11−13] Conventional antibiotics are a common treatment to prevent bacterial infections in diabetic wounds. Unfortunately, diabetic wounds have a longer healing cycle, and long-term antibiotic treatment increases the likelihood of the emergence of multidrug-resistant bacteria.[14] In previous reports, ROS provide an alternative approach to prevent bacterial infection and effectively reduce the potential to develop drug-resistant bacteria.[15] Therefore, supramolecular catalytic material is an important candidate to address diabetic wound infection. However, it is worth noting that diabetic wounds as chronic wounds with hyperglycemic environments and inflammatory environments[16] are quite susceptible to bacterial reinfection in the absence of wound dressings for protection. To date, supramolecular catalytic materials capable

Received: May 10, 2022
Accepted: June 9, 2022

Scheme 1. Step-by-Step Construction Process of the Supramolecular Cascade Reactor[a]

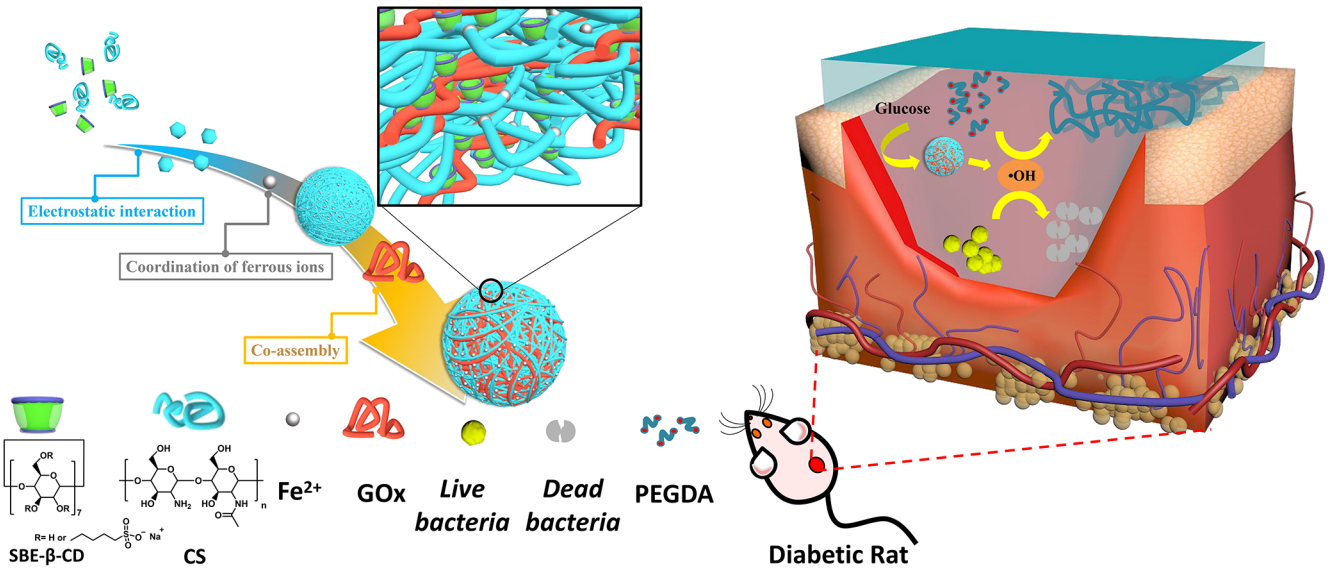

[a]Glucose activates the nanoconfinement supramolecular cascade reaction in diabetic chronic wounds, gelation *in situ* protection, and antibacterial processes.

of protecting wounds and potently eliminating drug-resistant bacterial infections have rarely been reported.

Herein, we report a "two birds with one stone" strategy to treat diabetic chronic wounds based on a supramolecular nanoconfined catalytic system. Specifically, the supramolecular cascade reactor was constructed by coassembly of chitosan (CS), sulfobutylether-β-cyclodextrin (SBE-β-CD), ferrous ions (Fe^{2+}), and glucose oxidase (GOx) through electrostatic and coordinative interactions.[17] The catalytic oxidation of glucose by GOx in a supramolecular cascade reactor provided H_2O_2 for the Fe^{2+}-mediated Fenton reaction, which finally generated ·OH. Then, ·OH generated by the glucose-activated cascade reaction was found to have a highly sterilizing effect on resistant bacteria *in vitro*. Importantly, with the mixed solution of poly(ethylene glycol) diacrylate (PEGDA) and glucose as the precursor solution, the supramolecular cascade reactor can further initiate radical polymerization and form a cross-linked polymer network hydrogel structure *in situ* on the wound while producing an antibacterial effect (Scheme 1). Significantly, the diabetic wound model demonstrated that the formation of hydrogels and the antibacterial effects of ·OH at the wound synergistically promoted the diabetic wound healing process. Thus, a glucose-activated nanoconfinement supramolecular cascade reaction *in situ* provides a highly efficient and facile cure method for diabetic chronic wounds.

RESULTS AND DISCUSSION

The construction process of the supramolecular cascade reactor was carried out in a stepwise manner, in which CS and SBE-β-CD served as the important constituent motifs of the reactor. Hence, the assembly process of CS and SBE-β-CD was explored in detail first. CS dissolved in acetic acid buffer (pH = 4.83), in which free amino groups were partly protonated, thus imparting a large positive charge on the molecular chains.[18] SBE-β-CD as an anionic water-soluble cyclodextrin derivative possesses the ability to form supramolecular assemblies with CS via electrostatic interactions.[19] To further determine the equivalent relationship between CS and SBE-β-CD in forming supramolecular assemblies, their critical aggregation concentrations (CACs) and preferable mixing ratios were determined by optical transmittance experiments (Figure 1a–d); CS and SBE-β-CD concentrations for generating supramolecular assemblies were deemed to be 20 μM:8 μg/L (SBE-β-CD/CS). In addition, the size and surface morphology of the supramolecular assemblies were tested by dynamic light scattering (DLS) and transmission electron microscopy (TEM), which revealed that the assemblies (CS@SBE-β-CD) formed nanoparticles (Figure S1a) with a size of approximately 54.3 nm (Figure 1g). Subsequently, the coordination between ferrous ions and amino groups in CS further promotes the formation of the CS@SBE-β-CD@Fe^{2+} process.[20] The characteristic peaks (at approximately 710.7 and 724.8 eV) of ferrous ions among CS@SBE-β-CD@Fe^{2+} can be observed by X-ray photoelectron spectroscopy (XPS) (Figure S2). The shifts change at 3100–3500, 1542–1660, and 1361–1475 cm^{-1} in the Fourier transform infrared spectroscopy (FT-IR) spectra (Figure 1f), and the appearance of an absorption peak at 338 nm in UV–vis absorption spectroscopy (Figure S3b) confirmed that ferrous ions coordinated with amino groups on CS. The formation process of CS@SBE-β-CD@Fe^{2+} promoted by ferrous ions was further observed and characterized by optical transmittance, DLS, zeta potential, and TEM. Compared with the CS@SBE-β-CD aqueous solution, the optical transmittance of the CS@SBE-β-CD@Fe^{2+} solution was decreased, and the Tyndall effect was enhanced (Figures 1e and S2a). The micromorphology also underwent the process from dispersed nanoparticles to fused nanospheres, and DLS results also confirmed the large increase in the size of the assemblies to 801 nm (Figures S1 and 1g). Interestingly, the change in the size and morphology of the assembly was accompanied by a change in the surface potential from negative (−2.3 mV) to positive (+13 mV) (Figure 1h). In addition, the loading efficiency of CS@SBE-β-CD-Fe^{2+} for ferrous ions was calculated to be 88.47% based on the hydroxylamine hydrochloride-*o*-phenanthroline system (Figure S4).[21]

https://doi.org/10.1021/acsnano.2c04566
ACS Nano XXXX, XXX, XXX–XXX

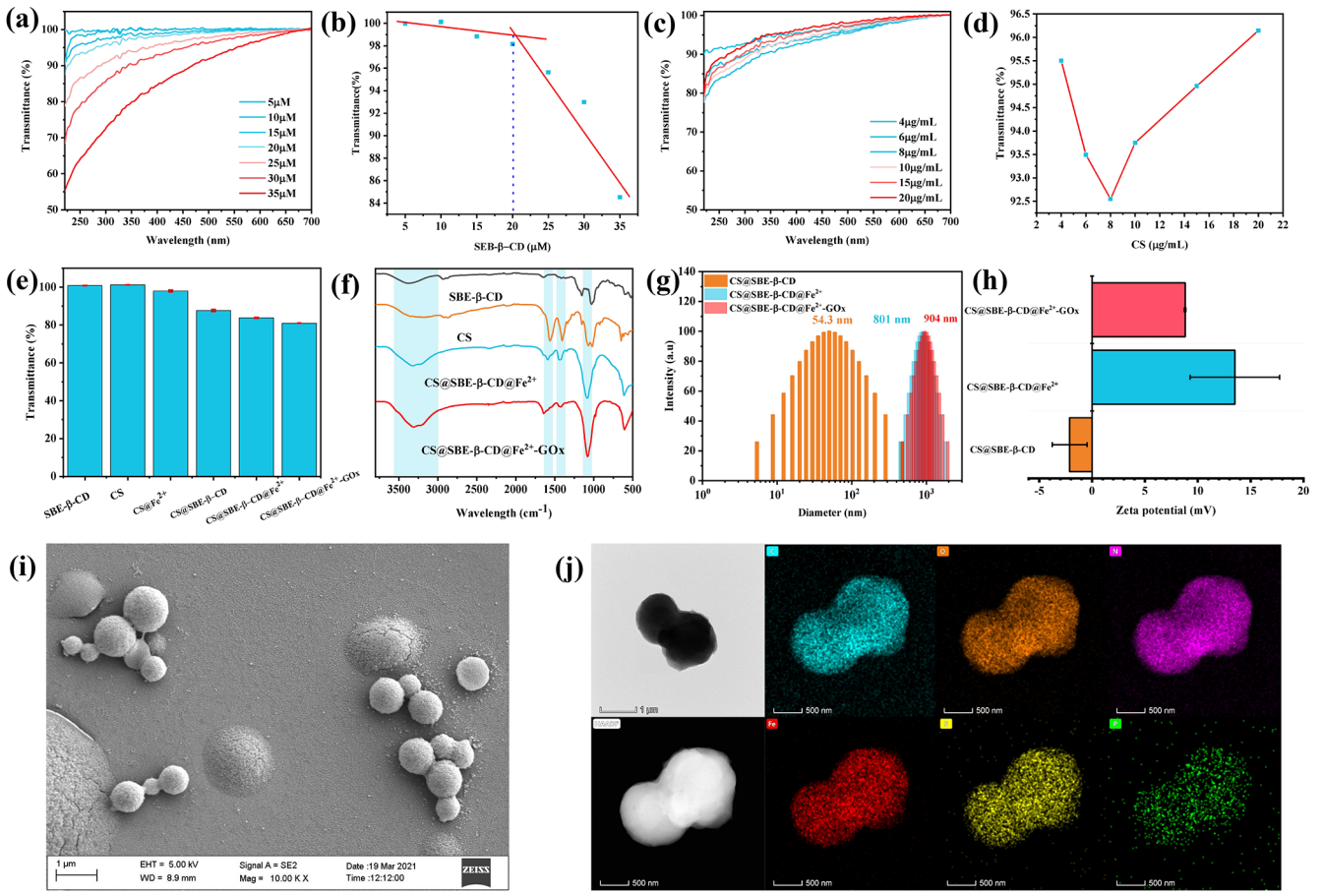

Figure 1. (a) Optical transmittance of SBE-β-CD and CS mixture aqueous solutions versus the SBE-β-CD concentration of aqueous solutions. (b) Optical transmittance at 400 nm of SBE-β-CD and CS mixture aqueous solutions as a function of SBE-β-CD concentration at 25 °C. (c) Optical transmittance of SBE-β-CD and CS mixture aqueous solutions versus the CS concentrations of aqueous solutions. (d) Optical transmittance at 400 nm of SBE-β-CD and CS mixture aqueous solutions as a function of CS concentration at 25 °C. (e) Optical transmittance changes of different components at 400 nm. The error is the standard deviation from the mean (n = 3). (f) Fourier transform infrared spectrograms of SBE-β-CD, CS, CS@SBE-β-CD@Fe^{2+}, and CS@SBE-β-CD@Fe^{2+}-GOx. (g) Dynamic light scattering results of CS@SBE-β-CD, CS@SBE-β-CD@Fe^{2+}, and CS@SBE-β-CD@Fe^{2+}-GOx. (h) Surface potentials of CS@SBE-β-CD, CS@SBE-β-CD@Fe^{2+}, and CS@SBE-β-CD@Fe^{2+}-GOx. The error is the standard deviation from the mean (n = 3). (i) SEM image of CS@SBE-β-CD@Fe^{2+}-GOx. (j) TEM image and EDS elemental mapping images of CS@SBE-β-CD@Fe^{2+}-GOx.

GOx, as the core part, forms the final supramolecular cascade reactor by coassembly with CS@SBE-β-CD-Fe^{2+}. The transmittance of the assembly solution was further reduced, and the FT-IR signal at around 3100−3500 cm^{-1} was further intensified by the introduction of GOx (Figure 1e). Moreover, the size and surface potential of the supramolecular assembly were further changed. The result shows that the size of the assembly increased from 801 to 904 nm, and the surface potential changed from 13.5 to 8.8 mV (Figure 1g,h). The final morphology of the nanoconfinement supramolecular cascade reactor (CS@SBE-β-CD-Fe^{2+}-GOx) was characterized by scanning electron microscopy (SEM) and TEM (Figures 1i,j and S6), which intuitively confirmed the spherical structure. Elemental mapping of C, O, N, Fe, S, and P (phosphorus comes from flavin adenine dinucleotide (FAD) in GOx) in CS@SBE-β-CD-Fe^{2+}-GOx indicated that GOx was successfully loaded into supramolecular assembly (Figure 1j). Quantitatively, the loading efficiency of the CS@SBE-β-CD-Fe^{2+}-GOx for GOx was calculated to be 22.9% based on the Bradford assay (Figure S5).[22]

The mechanism of the cascade reaction in CS@SBE-β-CD@Fe^{2+}-GOx is illustrated in Figure 2a. In brief, the GOx in the CS@SBE-β-CD@Fe^{2+}-GOx is activated by the substrate glucose to catalyze the process of the supramolecular cascade reaction, and the intermediate product (H_2O_2) further undergoes a Fenton reaction with Fe^{2+} to produce ·OH. To verify the cascade reaction process and its activation conditions, the 3,3′,5,5′-tetramethylbenzidine (TMB) assay was employed. TMB could be oxidized by ·OH generated by the cascade reaction to form blue oxTMB,[23] which could be monitored by UV−vis absorption spectroscopy and the naked eyes. As shown in Figures 2b and S7, the experiment results reveal that GOx is a component crucial for the generation of the cascade process, and the cascade could occur only when both the glucose substrate and the weak acid conditions were satisfied. Furthermore, the ·OH generated in the cascade reaction was captured by 5, 5-dimethyl-1-pyrrolidine-*N*-oxide (DMPO) and characterized by electron paramagnetic resonance (EPR). The characteristic EPR spectra for the DMPO−OH adducts with a 1:2:2:1 quadruple signal with aN = aH = 14.9 G were observed in Figure 2c.[24] This

https://doi.org/10.1021/acsnano.2c04566
ACS Nano XXXX, XXX, XXX−XXX

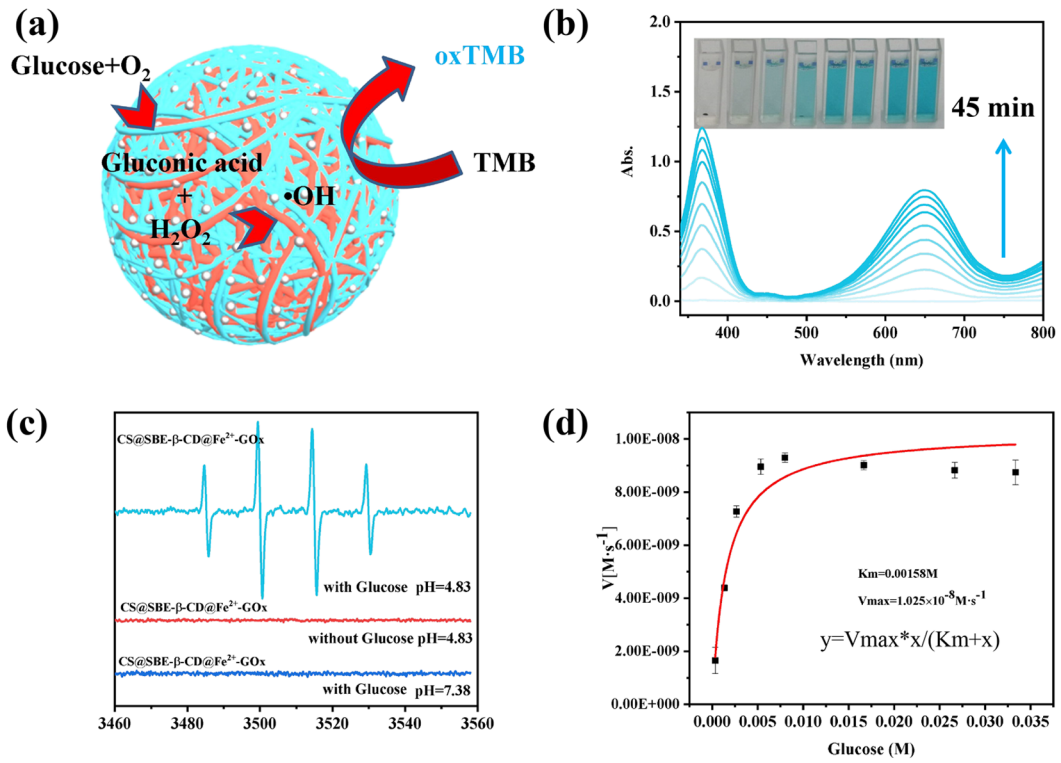

Figure 2. (a) Nanoconfinement supramolecular cascade reaction detected by the TMB chromogenic assay. (b) UV absorption of TMB changes in glucose aqueous solution with a supramolecular cascade reactor (pH = 4.83, [GOx] = 1.06 μg/mL, [Fe^{2+}] = 0.1 mM, [CS] = 0.8 μg/mL, [SBE-β-CD] = 2 × 10^{-6} M, [TMB] = 0.2 mM). (c) EPR spectrum of hydroxyl radicals produced by the cascade reaction of the supramolecular assembly under different conditions. (d) Steady-state kinetic assay of CS@SBE-β-CD@Fe^{2+}-GOx activity. The error is the standard deviation from the mean (n = 3) (Figure S8).

paramagnetic signal indicates that the cascade reaction produces hydroxyl radicals and further verifies the condition of the supramolecular cascade reaction.

The effect of CS@SBE-β-CD@Fe^{2+}-GOx on the activity of GOx was studied by the Michaelis−Menten kinetic model. Michaelis−Menten curves of natural free GOx and CS@SBE-β-CD@Fe^{2+}-GOx and the fitting parameters (K_m is the Michaelis−Menten constant, and V_{max} is the maximal reaction velocity) are shown in Figures 2d and S9). In contrast to the K_m and V_{max} of GOx, the parameters among CS@SBE-β-CD@Fe^{2+}-GOx all decrease, which implies that the supramolecular assemblies play the role of anticompetitive inhibitors of the enzymes.[25] It is speculated that the effect of the positive potential of the CS@SBE-β-CD@Fe^{2+}-GOx surface on the diffusion rate of the catalytic oxidation product gluconic acid may be the main reason leading to the above phenomenon. On the other hand, this result further confirms that the enzymes form supramolecular assemblies by coassembly. Notably, it was found that the formation of the supramolecular cascade reactor improved the stability of the enzyme in extreme environments (Figure S10a) as well as physiological conditions (Figure S10b). Further testing found that the supramolecular cascade reactor could maintain stable structures over a wide temperature range, so it was speculated that the noncovalent interactions in the assemblies can effectively prevent the spatial structure of GOx from changing and inactivating (Figure S10c).

The glucose-activated nanoconfinement supramolecular cascade reaction process has the ability to continuously produce ·OH. Hence, the antibacterial effect of the CS@SBE-β-CD@Fe^{2+}-GOx on drug-resistant bacteria was evaluated in detail. Gram-positive bacteria *S. aureus Xen36 and* Gram-negative bacteria *E. coli Xen14* were selected as drug-resistant bacteria representatives for testing. Glucose solution was added to the culture system to mimic hyperglycemic diabetic wounds (7.5 mM glucose). It was found that none of them produced obvious antibacterial activity against both *S. aureus Xen36* and *E. coli Xen14* in PBS, CS, SBE-β-CD, CS@SBE-β-CD, or CS@SBE-β-CD@Fe^{2+} by the minimum inhibitory concentration experiment. Only the CS@SBE-β-CD@Fe^{2+}-GOx showed a significant sterilizing effect in the hyperglycemic environment (Figure S11). The plate counting method further validated the above results (Figure S12). To further explore the antibacterial capability of the supramolecular cascade reactor, the micromorphology of two bacterial strains was examined by SEM after treatment with CS@SBE-β-CD@Fe^{2+}-GOx or a control component for 5 h in the hyperglycemic environment (Figures 3a, S13a, and S14a). Compared with the control, the CS@SBE-β-CD@Fe^{2+}-GOx produced a significant morphological collapse and cell wall dehiscence in the bacteria. Thus, the process of glucose-activated supramolecular cascade reaction to produce highly toxic ·OH for cell wall destruction may be the main cause of the bacterial killing. Further, live/dead bacteria were stained by STYO9/PI dyes and imaged by confocal laser scanning microscopy; the experimental results confirmed the efficient bacterial killing by the CS@SBE-β-CD@Fe^{2+}-GOx (Figures 3b, S13b, and S14b). In addition, the colony growth observed by the spread plate method is generally consistent with the tests described above (Figures 3c, S13c, and S14c).

https://doi.org/10.1021/acsnano.2c04566
ACS Nano XXXX, XXX, XXX−XXX

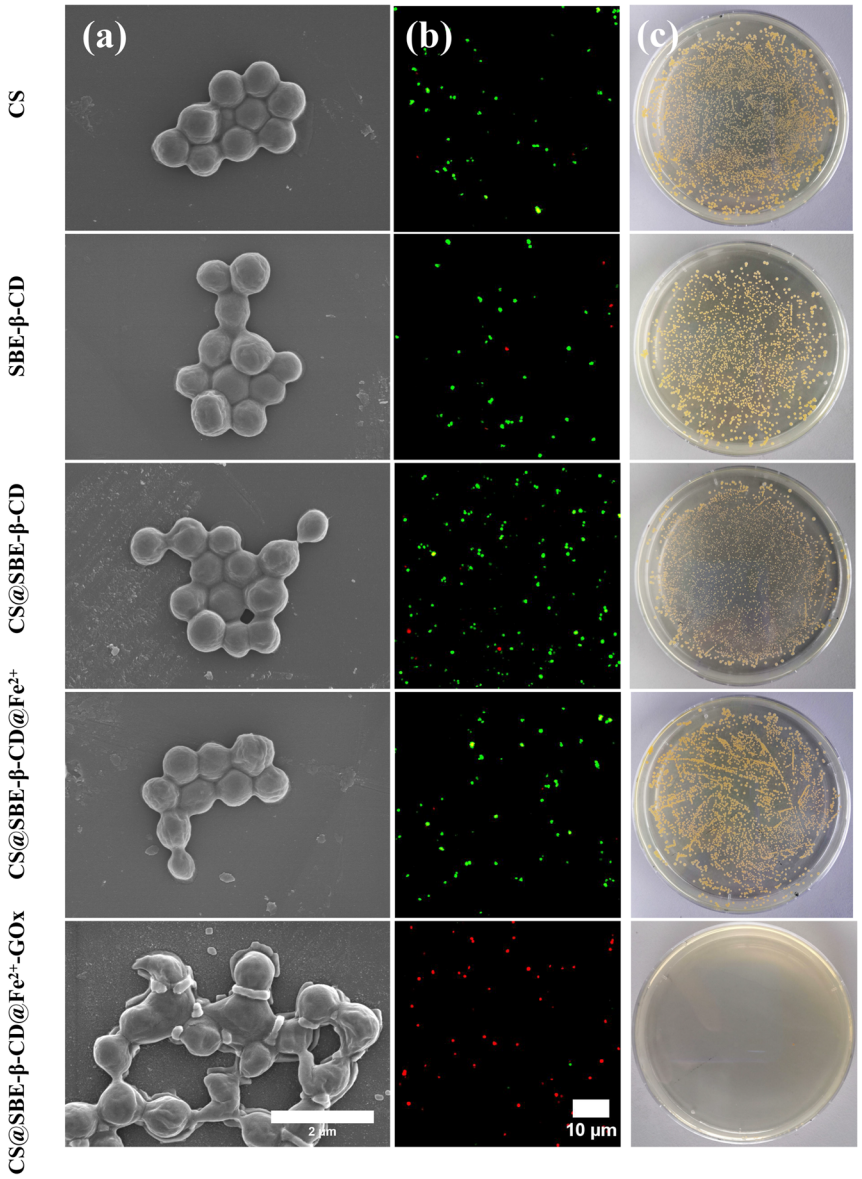

Figure 3. SEM images of *S. aureus Xen*36 (a), SYTO9/PI two-color fluorescent images of *S. aureus Xen*36 (b), and photographs of *S. aureus Xen*36 colonies (c) after treatment with different components for 5 h in a hyperglycemic environment (pH = 4.83, [Glu] = 7.5 mM, [GOx] = 10.6 μg/mL, [CS] = 8 μg/mL, [SBE-β-CD] = 2×10^{-5} M, [Fe^{2+}] = 1 mM).

During the experiment, it was found that ·OH generated by the supramolecular cascade reaction can rapidly initiate the polymerization of vinyl monomers (Figures S15 and S16).[26] To verify this process, four different kinds of vinyl monomers were chosen: poly(ethylene glycol) diacrylate (PEGDA400, PEGDA700), acrylamide (AM, with 3% bis-acrylamide (BIS)), *N*-vinyl-2-pyrrolidinone (NVP, 3% BIS), and *N*-isopropylacrylamide (NIPAM, 3% BIS). The rapid polymerization of monomers initiated by the nanoconfinement supramolecular cascade reaction to form hydrogels was tested by the tube inversion method (Figure S17).[27] Fortunately, when the monomer concentration was greater than 2 wt %, most monomers could be initiated to polymerize and form stable hydrogels (Table S1). It is worth noting that the system does not experience significant temperature fluctuations during the hydrogel formation (Figure S18). The mild gelation process implied that the occurrence of this process at the wound did not cause excessive pain. Furthermore, rheological experiment results showed that polymerization initiated by the supramolecular cascade reaction generated polymer gel network structures whose storage modulus could reach approximately 10^4 Pa (Figure S19).

As a kind of wound dressing with good biocompatibility, hydrogel has been widely used in wound protection and treatment.[28] Therefore, inspired by previous work. The above experimental results prompted us to apply CS@SBE-β-CD@Fe^{2+}-GOx to the diabetic wound treatment process. First, the stability as well as biocompatibility of the supramolecular cascade reactor under physiological conditions were systematically evaluated. The results reveal that the supramolecular cascade reactor is able to maintain a stable state at physiological ionic strength (0.154 mol/L) and exhibit negligible toxicity as well as hemolysis (Figure S20). Then, the Sprague−Dawley diabetic rat model was established by a streptozocin injection. A drug-resistant bacteria-infected chronic wound model was established by bioluminescent *S.*

https://doi.org/10.1021/acsnano.2c04566
ACS Nano XXXX, XXX, XXX−XXX

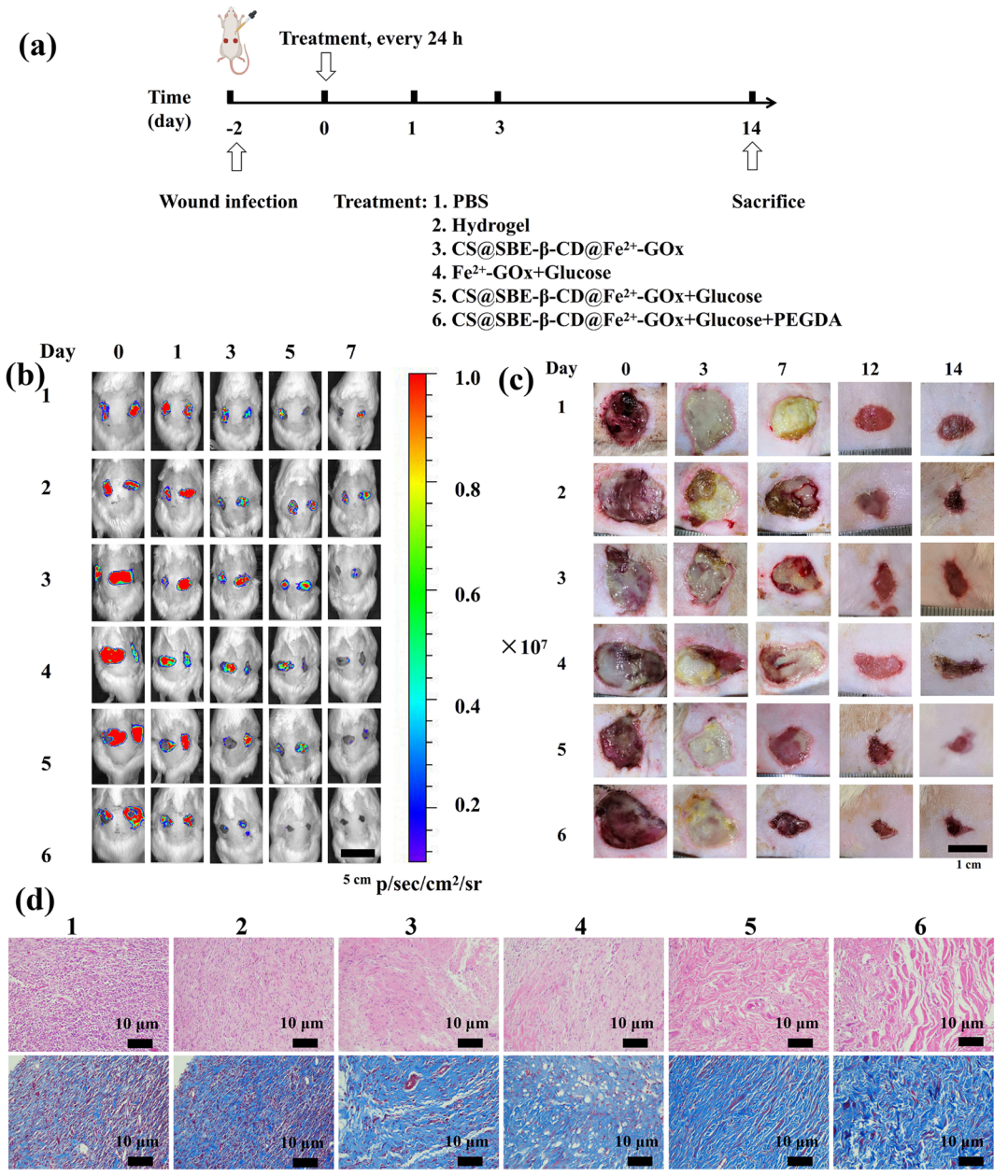

Figure 4. (a) Establishment of an animal model of a diabetes wound infected by *S. aureus Xen36* and its treatment process. (b) Bioluminescence images at wounds during treatment. (c) Photographs of wounds in an *S. aureus Xen36*-infected diabetic rat on different days. (d) Wound tissue staining analysis.

aureus Xen36-infected wounds.[29−32] Subsequently, 2 days after inducing infection, treatment was started with PBS, hydrogel, CS@SBE-*β*-CD@Fe^{2+}-GOx, Fe^{2+}-GOx + glucose, CS@SBE-*β*-CD@Fe^{2+}-GOx + glucose, or CS@SBE-*β*-CD@Fe^{2+}-GOx + glucose + PEGDA (Figure 4a). Here, PEGDA700 with good biocompatibility and degradability was selected as the monomer to construct the hydrogel.[33,34] To evaluate the sterilization effect of different components on *S. aureus Xen36*, the bioluminescent intensities in wounds were recorded starting 2 days after initiating infection using an IVIS Lumina XRMS Series III bio-optical imaging system (Figures 4b and S23a). Wound infection became evident from bioluminescent images. The results showed that CS@SBE-*β*-CD@Fe^{2+}-GOx + glucose + PEGDA have potent antimicrobial efficacy. In parallel, except the PBS group, all other groups showed a degree of antibacterial activity. Among them, the bactericidal effect of the hydrogel formed separately is far less than that of the hydrogel formed *in situ*, which may be caused by the short life of ·OH (<40 ns) and limited diffusion distance (about 10 nm).[35] Further, the healing process of diabetic wounds was recorded by photographs (Figure 4c). Notably, the rate of wound healing in the CS@SBE-*β*-CD@Fe^{2+}-GOx + glucose + PEGDA treatment was significantly faster than that of other treatment groups, and a significant reduction in wound area was observed within 7 days (Figure S23b). From the wound tissue sections stained with H&E and Masson (Figure 4d), wound tissue treated with CS@SBE-*β*-CD@Fe^{2+}-GOx + glucose + PEGDA has fewer inflammatory cells (Figure S23c) and stout collagen fibers, which indicated the nano-confinement supramolecular cascade reaction at the diabetes

https://doi.org/10.1021/acsnano.2c04566
ACS Nano XXXX, XXX, XXX−XXX

wound can significantly promote the process of wound healing.[36,37] The reason for the above phenomenon is speculated as follows: (1) Through the hydrogel (Figure S21), the CS@SBE-β-CD@Fe^{2+}-GOx can be tethered to the wound, making it available to consume the blood glucose in the wound for a sustained antibacterial effect and reduce the chance of reinfection (Figure S22). (2) Hydrogel formed *in situ* by a nanoconfinement supramolecular cascade reaction provides a closed and moist healing environment for the wound, benefits the formation of epithelial cells, promotes granulation tissue growth, and accelerates wound healing. Moreover, the CS@SBE-β-CD@Fe^{2+}-GOx had a negligible effect on the growth of rats during the treatment (Figure S23d).

CONCLUSION

In summary, we facilely and efficiently constructed a supramolecular cascade reactor for the treatment of diabetic chronic wounds. Under physiological conditions, the glucose-activated nanoconfinement supramolecular cascade reaction generates ·OH, which can also initiate free radical polymerization to form stable hydrogels after the introduction of PEGDA. *In vitro* experiments confirmed the obvious antibacterial effects of the ·OH generated from nanoconfinement supramolecular cascade reaction activated under a hyperglycemic environment. Notably, *in vivo* experiments confirmed that the nanoconfinement supramolecular cascade reaction process at the wound site could achieve antibacterial effects and hydrogel wound protection simultaneously, which significantly improved the healing process of diabetic chronic wounds. Overall, we successfully achieved hydrogel wound protection and combated drug-resistant bacterial infection through supramolecular catalytic material, and this strategy can also be applied to the study of complex diseases, such as *in situ* tumor therapy as well as cancer cell spreading inhibition.

EXPERIMENTAL SECTION

Materials. All solvents and reagents were commercially available and used without further purification unless noted otherwise. Sulfobutylether-β-cyclodextrin was purchased from Shandong Binzhou Zhiyuan Biotechnology Co., Ltd., and chitosan (deacetylation degree = 85%) was purchased from Heowns Biochemical Technology Co., Ltd. Absorption spectra were recorded on a Thermo Fisher Scientific EVO300 PC spectrophotometer in a conventional rectangular quartz cell (10 × 10 × 45 mm) at 25 °C. Transmission electron microscope (TEM) measurements were recorded on a high-resolution TEM (Tecnai G2 F20 microscope, FEI) equipped with a CCD camera (Orius 832, Gatan) operating at an accelerating voltage of 200 kV and with high-resolution transmission electron microscopy (HRTEM, FEI Talos F200X G2). Scanning electron microscope (SEM) measurements were recorded on cold field SEM (JSM-7500F). Live imaging measurements were recorded on an IVIS Lumina XRMS Series III (exposure time, 10s).

Preparation of Supramolecular Assemblies CS@SBE-β-CD. Chitosan (CS) was dissolved in acetic acid buffer solution (pH = 4.83, 0.1 M) with a concentration of 3 mg/mL. Sulfobutylether-β-cyclodextrin (SBE-β-CD) was dissolved in acetic acid buffer solution (pH = 4.83, 0.1 M) with a concentration of 3 mM. Then, the two were mixed in aqueous solution according to the preferable mixing ratios and ultrasonically mixed for 10 min to obtain the supramolecular assemblies CS@SBE-β-CD.

Preparation of Supramolecular Assemblies CS@SBE-β-CD@Fe^{2+}. CS (800 μL, 3 mg/mL, pH = 4.83), 2 mL of SBE-β-CD (3 mM, pH = 4.83), and 83.4 mg of $FeSO_4·7H_2O$ were added in deionized water, and the volume of the solution reached 30 mL. Subsequently, the mixture solution was purified by dialysis (molecular weight cut off 3500) in degassed water several times. The content of ferrous ions in the solution was monitored by the hydroxylamine hydrochloride-*o*-phenanthroline system.

Preparation of Supramolecular Assemblies CS@SBE-β-CD@Fe^{2+}-GOx. CS (120 μL, 3 mg/mL, pH = 4.83), 500 μL of GOx (1 mg/mL), 300 μL of SBE-β-CD (3 mM, pH = 4.83), and 12.5 mg of $FeSO_4·7H_2O$ were added in deionized water, and the volume of the solution reached 5 mL. Subsequently, the mixture solution was sonicated for 10 min and purified by dialysis (molecular weight cut off 100 000) in degassed water several times. The content of GOx in the solution was monitored by the Bradford assay. The solution in the dialysis tube is the supramolecular assembly solution.

Determination of Ferrous Ions in CS@SBE-β-CD@Fe^{2+}-GOx. Quantitative experiments of ferrous ions among the supramolecular assemblies were performed by the hydroxylamine hydrochloride-*o*-phenanthroline system. In brief, the content of ferrous ions inside the supramolecular assemblies was further determined by testing the amount of ferrous ions outside the dialysis tubing using a standard curve. The detailed calculation process is shown in Figure S4.

Determination of GOx in CS@SBE-β-CD@Fe^{2+}-GOx. Quantitative experiments of GOx among the supramolecular assemblies were performed by the Bradford assay. In brief, the content of GOx inside the supramolecular assemblies was further determined by testing the amount of GOx outside the dialysis tubing using a standard curve. The detailed calculation process is shown in Figure S5.

Measurement of the Supramolecular Cascade Reaction Process. The TMB method was used to evaluate the cascade reaction process of the supramolecular cascade reactor. The concentrations of the supramolecular cascade reactor were diluted 450-fold, and the concentrations of components in the assembly solution were as follows: [GOx] = 1.06 μg/mL, [CS] = 0.8 μg/mL, [SBE-β-CD] = 2×10^{-6} M, and [Fe^{2+}] = 0.1 mM.

Glucose (15 mM), 0.5 mL of acetic acid buffer solution (pH = 4.83, 0.1 M), 0.5 mL of CS@SBE-β-CD@Fe^{2+}-GOx solution, and 20 μL of TMB (0.03 M in DMSO) were mixed together and brought to a final volume of 3 mL with the addition of deionized water. During the reaction, the absorbance change was monitored by UV−vis spectroscopy.

***In Vitro* Antibacterial Activity of Supramolecular Cascade Reactor.** The concentrations of each component in the supramolecular cascade reactor used for antibacterial experiments were [GOx] = 10.6 μg/mL, [CS] = 8 μg/mL, [SBE-β-CD] = 2×10^{-5} M, and [Fe^{2+}] = 1 mM.

To evaluate the bacteriostatic effect of CS@SBE-β-CD@Fe^{2+}-GOx in a liquid medium, solutions of six different compositions (PBS, CS, SBE-β-CD, CS@SBE-β-CD, CS@SBE-β-CD@Fe^{2+}, and CS@SBE-β-CD@Fe^{2+}-GOx separately) were mixed with the bacterial suspension. After 24 h of incubation, the absorbance of solutions at 600 nm was recorded. For the plate counting method, after incubation for different composition intervals up to 5 h at 37 °C, 10 μL aliquots were taken, serially diluted and plated on agar, and incubated for 24 h at 37 °C, after which the number of CFUs formed was determined. The silicon wafer was treated with piranha solution, and it was placed on a 24-well plate. After the six components were cocultured with the bacterial suspension in a well plate for 5 h, the supernatant was carefully removed, and 5% formaldehyde was added to fix the bacterial morphology for 1 h. Then, the bacteria were further dehydrated through 30, 50, 70, 90, and 100% ethanol solutions.

***In Vivo* Treatment of MRSA-Infected Diabetic Wounds.** To examine the therapeutic effects of the cascade reaction process of the supramolecular cascade reactor on actual diabetic wounds, we implemented the following animal experiments. Sprague−Dawley rats (weighing 220−240 g, male) were purchased from Beijing Weitonglihua Experimental Animal Technology Co., Ltd. The diabetic mice model was constructed by intraperitoneal injection of streptozocin (STZ). Diabetic chronic wound models infected with *S. aureus Xen36* were next established using diabetic mice. A pair of 1.5 cm diameter wounds were cut on the back of each rat and infected by dropwise addition of *S. aureus Xen36* solution (100 μL of each wound,

https://doi.org/10.1021/acsnano.2c04566
ACS Nano XXXX, XXX, XXX−XXX

1×10^9 CFU/mL). The animal experiment was approved by the Animal Protection and Utilization Committee of the Institute of Radiology, Chinese Academy of Medical Sciences.

Rat with diabetic chronic wounds was divided into six groups for testing.

Group 1 samples: The blank group received PBS solution dropwise at the wound every 24 h.

Group 2 samples: Hydrogels were formed in tubes by mixing solutions of 200 μL of glucose-acetic acid buffer solution containing PEGDA700 ([PEGDA700] = 12 wt %) and 200 μL of CS@SBE-β-CD@Fe^{2+}-GOx solution. Then, hydrogels were fixed to the wound by 3 M gas permeable adhesive tape. The hydrogel was changed every 24 h.

Group 3 samples: 200 μL of acetic acid buffer solution and 200 μL of CS@SBE-β-CD@Fe^{2+}-GOx solution were added to the wound every 24 h.

Group 4 samples: 200 μL of glucose-acetic acid buffer solution ([glucose] = 15 mM) and 200 μL of Fe^{2+}-GOx solution were added to the wound every 24 h.

Group 5 samples: 200 μL of glucose-acetic acid buffer solution ([glucose] = 15 mM) and 200 μL of CS@SBE-β-CD@Fe^{2+}-GOx solution were added to the wound every 24 h.

Group 6 samples: 200 μL of glucose-acetic acid buffer solution containing PEGDA700 ([PEGDA700] = 12 wt %) and 200 μL of CS@SBE-β-CD@Fe^{2+}-GOx solution were added to the wound every 24 h, and the mixed solution at the wound site formed hydrogels *in situ* about 3 min later.

Histological Analysis. All wound specimens were fixed in 4% formaldehyde solution for 2∼3 days and then embedded in paraffin to prepare 3−4 μm thick tissue sections. Tissue sections were stained with H&E/Masson and imaged under an optical microscope.

ASSOCIATED CONTENT

Supporting Information

The Supporting Information is available free of charge at https://pubs.acs.org/doi/10.1021/acsnano.2c04566.

Preparation process, component characterization, component quantitative analysis, and reaction condition experiment of the supramolecular cascade reactor (Figures S1−S6). Condition exploration of the supramolecular cascade reaction process activated by glucose (Figures S7−S9). Stability test of the supramolecular cascade reactor (Figure S10). *In vitro* antibacterial performance test of the supramolecular cascade reactor (Figures S11−S14). Experimental process of *in situ* gelation initiated by supramolecular cascade reaction (Figures S15−S19 and Table S1). Biocompatibility test of the supramolecular cascade reactor (Figure S20). Pictures of the wound treatment process of diabetes (Figure S21). SEM image of the hydrogel at the wound (Figure S22). Quantitative data assessment during in vivo wound treatment (Figure S23) (PDF)

AUTHOR INFORMATION

Corresponding Author

Yu Liu − *College of Chemistry, State Key Laboratory of Elemento-Organic Chemistry, Nankai University, Tianjin 300071, P. R. China; Haihe Laboratory of Sustainable Chemical Transformations, Tianjin 300192, P. R. China; Collaborative Innovation Center of Chemical Science and Engineering (Tianjin), Tianjin 300072, P. R. China;* orcid.org/0000-0001-8723-1896; Email: yuliu@nankai.edu.cn

Authors

Lei Chen − *College of Chemistry, State Key Laboratory of Elemento-Organic Chemistry, Nankai University, Tianjin 300071, P. R. China; Oujiang Laboratory (Zhejiang Lab for Regenerative Medicine, Vision and Brain Health), Wenzhou Institute, University of Chinese Academy of Sciences, Wenzhou 325001, P. R. China*

Yong Chen − *College of Chemistry, State Key Laboratory of Elemento-Organic Chemistry, Nankai University, Tianjin 300071, P. R. China*

Rong Zhang − *College of Chemistry, State Key Laboratory of Elemento-Organic Chemistry, Nankai University, Tianjin 300071, P. R. China*

Qilin Yu − *Key Laboratory of Molecular Microbiology and Technology, Ministry of Education, College of Life Sciences, Nankai University, Tianjin 300071, P. R. China;* orcid.org/0000-0003-0473-5111

Yong Liu − *Oujiang Laboratory (Zhejiang Lab for Regenerative Medicine, Vision and Brain Health), Wenzhou Institute, University of Chinese Academy of Sciences, Wenzhou 325001, P. R. China;* orcid.org/0000-0003-1738-7857

Complete contact information is available at: https://pubs.acs.org/10.1021/acsnano.2c04566

Notes

The authors declare no competing financial interest.

ACKNOWLEDGMENTS

This work was financially supported by the National Natural Science Foundation of China (grants 22131008). We thank the Haihe Laboratory of Sustainable Chemical Transformations for financial support. Figure 4a was created with BioRender.com.

REFERENCES

(1) Gupta, S.; Chattopadhyay, T.; Pal Singh, M.; Surolia, A. Supramolecular insulin assembly II for a sustained treatment of type 1 diabetes mellitus. *Proc. Natl. Acad. Sci. U. S. A.* **2010**, *107*, 13246−13251.

(2) Maikawa, C. L.; Smith, A. A. A.; Zou, L.; Roth, G. A.; Gale, E. C.; Stapleton, L. M.; Baker, S. W.; Mann, J. L.; Yu, A. C.; Correa, S.; Grosskopf, A. K.; Liong, C. S.; Meis, C. M.; Chan, D.; Troxell, M.; Maahs, D. M.; Buckingham, B. A.; Webber, M. J.; Appel, E. A. A co-formulation of supramolecularly stabilized insulin and pramlintide enhances mealtime glucagon suppression in diabetic pigs. *Appel. Nat. Biomed. Eng.* **2020**, *4*, 507−517.

(3) Zuo, M.; Qian, W.; Xu, Z.; Shao, W.; Hu, X. Y.; Zhang, D.; Jiang, J.; Sun, X.; Wang, L. Multiresponsive Supramolecular Theranostic Nanoplatform Based on Pillar[5]arene and Diphenylboronic Acid Derivatives for Integrated Glucose Sensing and Insulin Delivery. *Small* **2018**, *14*, No. 1801942.

(4) Cheng, H.-B.; Zhang, Y.-M.; Liu, Y.; Yoon, J. Turn-On Supramolecular Host-Guest Nanosystems as Theranostics for Cancer. *Chem.* **2019**, *5*, 553−574.

(5) Li, X.; Lee, S.; Yoon, J. Supramolecular photosensitizers rejuvenate photodynamic therapy. *Chem. Soc. Rev.* **2018**, *47*, 1174−1188.

(6) Liu, Y. H.; Zhang, Y. M.; Yu, H. J.; Liu, Y. Cucurbituril-Based Biomacromolecular Assemblies. *Angew. Chem., Int. Ed.* **2021**, *60*, 3870−3880.

(7) Zhang, Y. M.; Liu, Y. H.; Liu, Y. Cyclodextrin-Based Multistimuli-Responsive Supramolecular Assemblies and Their Biological Functions. *Adv. Mater.* **2020**, *32*, No. 1806158.

(8) Xu, B.; Wang, H.; Wang, W.; Gao, L.; Li, S.; Pan, X.; Wang, H.; Yang, H.; Meng, X.; Wu, Q.; Zheng, L.; Chen, S.; Shi, X.; Fan, K.; Yan, X.; Liu, H. A Single-Atom Nanozyme for Wound Disinfection Applications. *Angew. Chem., Int. Ed.* **2019**, *58*, 4911−4916.
(9) Wang, M.; Zhou, X.; Li, Y.; Dong, Y.; Meng, J.; Zhang, S.; Xia, L.; He, Z.; Ren, L.; Chen, Z.; Zhang, X. Triple-synergistic MOF-nanozyme for efficient antibacterial treatment. *Bioact. Mater.* **2022**, *17*, 289−299.
(10) Liu, X. P.; Yan, Z. Q.; Zhang, Y.; Liu, Z. W.; Sun, Y. H.; Ren, J. S.; Qu, X. G. Two-Dimensional Metal-Organic Framework/Enzyme Hybrid Nanocatalyst as a Benign and Self-Activated Cascade Reagent for in Vivo Wound Healing. *ACS. Nano.* **2019**, *13*, 5222−5230.
(11) Muller, M.; Trocme, C.; Lardy, B.; Morel, F.; Halimi, S.; Benhamou, P. Y. Matrix metalloproteinases and diabetic foot ulcers: the ratio of MMP-1 to TIMP-1 is a predictor of wound healing. *Diabet. Med.* **2008**, *25*, 419−426.
(12) Armstrong, D. G.; Boulton, A. J.M.; Bus, S. A. Diabetic Foot Ulcers and Their Recurrence. *N. Engl. J. Med.* **2017**, *376*, 2367−2375.
(13) Malone-Povolny, M. J.; Maloney, S. E.; Schoenfisch, M. H. Nitric Oxide Therapy for Diabetic Wound Healing. *Adv. Healthc. Mater.* **2019**, *8*, No. 1801210.
(14) Blair, J. M.; Webber, M. A.; Baylay, A. J.; Ogbolu, D. O.; Piddock, L. J. Molecular mechanisms of antibiotic resistance. *Nat. Rev. Microbiol.* **2015**, *13*, 42−51.
(15) Yu, H. Z.; Li, X.; Xu, F.; Hu, X. L.; Yan, J.; Kwon, N.; Chen, G. R.; Tang, T.; Dong, X.; Mai, Y.; Chen, D.; Yoon, J.; He, X. P.; Tian, H. A Supramolecular-Based Dual-Wavelength Phototherapeutic Agent with Broad-Spectrum Antimicrobial Activity Against Drug-Resistant Bacteria. *Angew. Chem., Int. Ed.* **2020**, *59*, 3658−3664.
(16) Velander, P.; Theopold, C.; Hirsch, T.; Bleiziffer, O.; Zuhaili, B.; Fossum, M.; Hoeller, D.; Gheerardyn, R.; Chen, M.; Visovatti, S.; Svensson, H.; Yao, F.; Eriksson, E. Impaired wound healing in an acute diabetic pig model and the effects of local hyperglycemia. *Wound. Repair. Regen.* **2008**, *16*, 288−293.
(17) Zhang, Y.; Liu, Y. Supramolecular Assemblies of Multi-Charged Cyclodextrins. *Chinese. J. Org. Chem.* **2020**, *40*, 3802−3811.
(18) Liu, H. X.; et al. Determination of Nitrite and Nitrate in Dairy Products by Protonated Chitosan Functionalized Gold Nanoarticles Coated Stir Bar Sorptive Extraction with Ion Chromatography. *Chinese. J. Anal. Chem.* **2019**, *47*, 1395−1401.
(19) Chen, X. M.; Chen, Y.; Hou, X.-F.; Wu, X.; Gu, B.-H.; Liu, Y. Sulfonato-*β*-Cyclodextrin Mediated Supramolecular Nanoparticle for Controlled Release of Berberine. *ACS. Appl. Mater. Interfaces.* **2018**, *10*, 24987−24992.
(20) Gao, M. F.; et al. Degradation of methylene blue in a heterogeneous Fenton reaction catalyzed by chitosan crosslinked ferrous complex. *J. Taiwan. Inst. Chem. E* **2016**, *67*, 355−361.
(21) Wang, J.; Liu, H.; Liu, Y.; Chu, C.; Yang, Y.; Zeng, Y.; Zhang, W.; Liu, G. Eumelanin-Fe_3O_4 hybrid nanoparticles for enhanced MR/PA imaging-assisted local photothermolysis. *Biomater. Sci.* **2018**, *6*, 586−595.
(22) Bradford, M. A rapid and sensitive method for the quantitation of microgram quantities of protein utilizing the principle of protein-dye binding. *Anal. Biochem.* **1976**, *72*, 248−254.
(23) Chen, L.; Chen, Y.; Zhang, Y.; Liu, Y. Photo-Controllable Catalysis and Chiral Monosaccharide Recognition Induced by Cyclodextrin Derivatives. *Angew. Chem., Int. Ed.* **2021**, *60*, 7654−7658.
(24) Chen, L.; Chen, Y.; Fu, H. G.; Liu, Y. Reversible Emitting Anti-Counterfeiting Ink Prepared by Anthraquinone-Modified beta-Cyclodextrin Supramolecular Polymer. *Adv. Sci.* **2020**, *7*, 2000803.
(25) Dodgson, K. S.; Spencer, B.; Williams, K. Examples of anti-competitive inhibition. *Nature* **1956**, *177*, 432−433.
(26) Ye, Y.; Xiao, L.; He, B.; Zhang, Q.; Nie, T.; Yang, X.; Wu, D.; Cheng, H.; Li, P.; Wang, Q. Oxygen-tuned nanozyme polymerization for the preparation of hydrogels with printable and antibacterial properties. *J. Mater. Chem. B* **2017**, *5*, 1518−1524.
(27) Zhang, Y.; Liang, L.; Chen, Y.; Chen, X. M.; Liu, Y. Construction and Efficient Dye Absorption of Supramolecular Hydrogels by Cyclodextrin Pseudorotaxane and Clay. *Soft Mater.* **2019**, *15*, 73−77.
(28) Ouyang, J.; Ji, X. Y.; Zhang, X. C.; Feng, C.; Tang, Z. M.; Kong, N.; Xie, A.; Wang, J. Q.; Sui, X. B.; Deng, L.; Liu, Y. N.; Kim, J. S.; Cao, Y. H.; Tao, W. In situ sprayed NIR-responsive, analgesic black phosphorus-based gel for diabetic ulcer treatment. *Proc. Natl. Acad. Sci. U. S. A.* **2020**, *117*, 28667−28677.
(29) Liu, Y.; Busscher, H. J.; Zhao, B.; Li, Y.; Zhang, Z.; van der Mei, H. C.; Ren, Y.; Shi, L. Surface-Adaptive, Antimicrobially Loaded, Micellar Nanocarriers with Enhanced Penetration and Killing Efficiency in Staphylococcal Biofilms. *ACS Nano* **2016**, *10*, 4779−4789.
(30) Armstrong, D. G.; Lavery, L. A.; Harkless, L. B. Validation of a Diabetic Wound Classification System: The contribution of depth, infection, and ischemia to risk of amputation. *Diabetes Care.* **1998**, *21*, 855−859.
(31) Zhao, Y.; Li, Z.; Song, S.; Yang, K.; Liu, H.; Yang, Z.; Wang, J.; Yang, B.; Lin, Q. Skin-Inspired Antibacterial Conductive Hydrogels for Epidermal Sensors and Diabetic Foot Wound Dressings. *Adv. Funct. Mater.* **2019**, *29*, 1901474.
(32) King, A. J. The use of animal models in diabetes research. *Br J Pharmacol.* **2012**, *166*, 877.
(33) Freedman, B. R.; Uzun, O.; Luna, N. M. M.; Rock, A.; Clifford, C.; Stoler, E.; Ostlund-Sholars, G.; Johnson, C.; Mooney, D. J. Degradable and removable tough adhesive hydrogels. *Adv. Mater.* **2021**, *33*, No. 2008553.
(34) Huang, H.; Wang, X.; Wang, W.; Qu, X.; Song, X.; Zhang, Y.; Zhong, L.; Yang, D. P.; Dong, X.; Zhao, Y. Injectable hydrogel for postoperative synergistic photothermal-chemodynamic tumor and anti-infection therapy. *Biomaterials* **2022**, *280*, 121289.
(35) Li, X.; Bai, H.; Yang, Y.; Yoon, J.; Wang, S.; Zhang, X. Supramolecular antibacterial materials for combatting antibiotic resistance. *Adv. Mater.* **2019**, *31*, No. 1805092.
(36) Wang, Y.; Gao, D.; Liu, Y.; Guo, X.; Chen, S.; Zeng, L.; Ma, J.; Zhang, X.; Tian, Z.; Yang, Z. Immunogenic-cell-killing and immunosuppression-inhibiting nanomedicine. *Bioact. Mater.* **2021**, *6*, 1513−1527.
(37) Kim, W. Y.; Won, M.; Koo, S.; Zhang, X.; Kim, J. S. Mitochondrial H_2Sn-mediated anti-inflammatory theranostics. *Nano-micro. Lett.* **2021**, *13*, 168−181.

https://doi.org/10.1021/acsnano.2c04566
ACS Nano XXXX, XXX, XXX−XXX